Role of electrons in collision cascades in solids. I. Dissipative model

M. Caro,[1] A. Tamm,[2,*] A. A. Correa,[2,†] and A. Caro[3]
[1]*Department of Mechanical Engineering, Virginia Polytechnic Institute, Falls Church, Virginia 22043, USA*
[2]*Quantum Simulations Group, Lawrence Livermore National Laboratory, Livermore, California 94550, USA*
[3]*College of Professional Studies, George Washington University, Ashburn, Virginia 20147, USA*

(Received 10 December 2018; published 7 May 2019)

We present a detailed model for the nonadiabatic coupling between ions and electrons in energetic ion-solid interactions over a wide range of energies in concentrated solid-solution fcc alloys of the 3*d* transition metals Ni, Co, Fe, and Cr. The model is based on general statistical mechanical principles and results in a stochastic modification of the classical nuclei motion which is parameterized by the first-principles calculation of a dissipation function produced by explicit time-dependent electronic evolution. This model provides a full picture of an entire collision process, from the ballistic to the thermal phases of a cascade, giving a detailed description of the energy exchange between ions and electrons till their final thermalization, removing in this way some *ad hoc* assumptions used in the state-of-the-art atomistic two-temperature models. This work is separated in two papers; in the present Part I, we report on the *ab initio* methodology used to translate stopping power and electron-phonon interaction into a parameterized dissipation function; Part II, to be published, addresses the nonadiabatic ion dynamics using our modified Langevin dynamics [Tamm *et al.* Phys. Rev. Lett. **120**, 185501 (2018)] applying the dissipation functions developed here to specific collision cascade events.

DOI: 10.1103/PhysRevB.99.174301

I. INTRODUCTION

The traditional way to study the dynamics of ions in solids, and in particular the interaction of energetic ions with matter, relies on the Born-Oppenheimer approximation (BOA) [1], where ions and electrons can be decoupled and their equations of motion solved separately. An additional approximation, which considers that ions move classically under the forces derived from a potential energy function [e.g., the instantaneous ground state (GS) electronic energy], proves to be useful to describe both thermal motion and nuclear stopping power, S_n. However, for ion velocities approaching a fraction of the Fermi velocity of electrons in a solid target, electronic losses, or nonadiabatic effects, become increasingly relevant.

The rate of energy transfer to electrons can be cast in the form of an electronic inelastic cross section, leading to an electronic stopping power. As a simple extension of the BOA, S_n and S_e are customarily assumed to be independent of each other; however, in the presence of nonadiabatic energy exchange, the actual material response is considerably beyond the BOA [2] and the combined scattering of ions and electrons needs to be taken into account.

There is a vast literature reporting decades of theoretical and experimental work related to S_n and S_e, which started a century ago with Bohr at the time of the formulation of quantum mechanics [3–6] and extends to today; for a summary of the key discoveries, see the recent review by P. Sigmund [7].

Ion-solid interaction models for S_n in the adiabatic or elastic framework are based on the knowledge of the adiabatic potential energy function for ions, U_{adiab}, which enables the calculation of cross sections and S_n within classical mechanics using binary collisions theory. Seminal work addressing this problem by Lindhard *et al.* in the 1960s, known as the Lindhard-Scharff-Schiøtt (LSS) theory [8–11], provides a simple universal expression for the nuclear-scattering cross section with only a few parameters, such as the charges of projectile Z_1 and target Z_2 atoms. This universal description is achieved once a model for the screening of the nuclear charge by electrons is adopted, for example Thomas-Fermi theory, and translates into a nuclear stopping power that shows a maximum and tends to zero at low and high energies.

More recently, with the increase in computer power and accurate interatomic potentials, stopping power, range, and microscopic details of the ensuing damage could be obtained via full many-body ion-ion interactions within the frame of molecular dynamics that, for a given potential and within the realm of classical mechanics, provides the solution of the many-body interaction process; for a detailed discussion see Was [12].

Models for S_e fundamentally need to resort to quantum mechanics and yet were developed much earlier than those for S_n by Bohr, Bethe, Moller, Bloch, Lindhard, and others, as summarized in a 1963s review by Fano [13]. Electronic stopping power is characterized by a curve that has a maximum as a function of velocity, often called Bragg maximum, which occurs at a projectile velocity comparable with the characteristic velocity of electrons in the target, such as the Fermi velocity in an electron gas. Regimes of low or high energy refer to energies below or above this maximum, and are described by the Bethe (high energy) and Fermi-Teller [14] (low energy) approximate theories (see Ref. [7]). The intermediate regime has been a challenge for theoreticians, as

*Corresponding author: tamm3@llnl.gov
†Corresponding author: correaa@llnl.gov

is the very low-energy regime where band structure for solids [15,16] deviate from the results obtained for the uniform electron gas, introducing, for example, stopping power threshold effects in insulators [17].

Electronic stopping in the low-energy regime was studied using several theoretical approaches, most notably by Firsov [18] and the LSS theory [8]. These studies led to the characterization of S_e as a frictionlike force proportional to the projectile velocity.

The separation of scattering processes into elastic scattering and electronic stopping has been a dominating principle in ion-solid interaction physics for over 50 years. All Monte Carlo and binary-collision simulation codes were built on this principle. The popular transport of ions in matter (TRIM) code [19], and its extension incorporating stopping cross sections for energies above the stopping maximum, stopping and range of ions in matter (SRIM) [20], are basically an implementation of the LSS theory with a modified universal potential.

Lindhard's and Firsov's expressions for S_e for energies below the maximum predict velocity-proportional frictionlike stopping and, since originating in the Thomas-Fermi model, suggest a smooth dependence of the stopping cross section on Z_1 and Z_2. However, measurements by Ormrod and Duckworth for a series of ions in carbon [21] first showed Z_1 oscillations in electronic stopping cross sections, unaccounted for in those theories. The phenomenon was a manifestation of the electronic shell structure of the scattering centers, highlighting the need for more accurate descriptions of the electronic structure of projectiles and targets.

From the mid '80s, atomic-scale computer simulations presented a substantial leap in the predictive power of radiation damage studies, providing the most detailed picture of this process, with information usually much richer than experimentally accessible. Direct computer simulations of atomic motion and electron dynamics, a "brute force" approach, allows solving models whose complexity prevents analytical alternatives. It makes it possible to study ion-solid interaction directly from first principles, going significantly beyond effective theories. A fully atomistic first-principles calculation of electronic stopping for a wide range of projectile velocities has only recently been possible [2,22–28]. These recent advances rely on nonperturbative time-dependent density functional theory (TDDFT) [29].

The computational resources required by this first-principles approach prevent its use in cases where the ion dynamics needs to be followed over much longer time scales, e.g., picoseconds, or to study defect creation following cascades. For those cases, the state of the art in computer simulations for the combined ion and electron dynamics in the nonadiabatic picture is molecular dynamics (MD) with empirical potentials for the ions, and the continuum heat diffusion equation for the electrons. The two systems are connected via electron-ion coupling terms extracted from the *ab initio* theories, in what is termed atomistic two-temperature models, TTMs [30–32].

The parametrization of quantum mechanical results to feed classical equations of motion for the ions has a long history of accomplishments, the most successful being the one leading to SRIM, as mentioned earlier [20]. In the framework of MD, the use of Langevin equations with a damping term as a function of the local electronic density was proposed by one of us in the '80s [33] as a plausible model of the two-temperature system.

More recently, we showed that TDDFT not only gives quantitatively accurate values for the stopping power regime [34], but also for the electron-phonon interaction regime when seen as a stopping process for energies in the meV range [35]. TDDFT and Ehrenfest forces [36] were used to calculate the electronic excitations and dissipation produced by a moving Ni ion in a Ni crystal in the MeV range (electronic stopping power regime), as well as thermal energy meV range (electron-phonon interaction regime). Generally, results at high energy compare well to experimental databases of stopping power, and those at low energy are very similar to linear response calculations when applicable, and experimental measurements. This approach to electron-phonon interaction as an electronic stopping process provides the basis for a unified framework to perform classical molecular dynamics of ion-solid interaction with *ab-initio*-derived nonadiabatic terms in a wide range of energies.

The purpose of this paper is to provide a first-principles approach to ion-electron interaction in concentrated alloys for MD applications, and is motivated by recent evidence showing that the way radiation energy is deposited into the lattice in concentrated solutions, and later transported away, plays a significant role in the early stages of radiation damage [37]. While it has been shown that disorder significantly affects transport within the electronic and ionic systems, its effects on the interaction between the two subsystems has not yet been elucidated. The materials of interest for our paper are the face-centered cubic (fcc) concentrated solid solutions based on Ni and its neighbors in the 3*d* transition metal series, namely Co, Fe, and Cr.

This paper is organized as follows. Section II describes the model. In Sec. III, we describe the first-principles theory and simulation methods we use; Sec. IV describes the construction of the dissipation function; Sec. V contains the Discussion and Summary of the paper.

II. MODEL

The model for the role of electrons in energetic ion-solid interactions proposed in this paper is based on our generalized Langevin framework [38] for classical MD, where we replace the scalar values of friction and random forces over individual particles with many-body forces that act in a *correlated* manner over different particles, called here EPH-MD (electron phonon-molecular dynamics) [39]. This represents a realistic bathlike interaction with electrons by a friction term [40,41] for electronic stopping power and e-ph interaction, and a random force, e.g., produced by electronic fluctuations). In this model, the force on particle I has three contributions:

$$\mathbf{f}_I = -\nabla_I U_{\text{adiab}} - \sum_J \mathsf{B}_{IJ}\mathbf{v}_J + \sum_J \mathsf{W}_{IJ}\boldsymbol{\xi}_J. \qquad (1)$$

The first term represents the conservative forces, assumed here to be independent of the electronic excitations. The second and third terms are the friction and random forces of

the generalized Langevin dynamics, where the random forces are correlated, as made explicit by the tensor notation.

A model for ionic motion that equilibrates with a thermal bath (electrons) at a locally smooth temperature T_e must fulfill several conditions: First, $\{\xi_I\}_I$ must be white-noise and mutually uncorrelated Gaussian random variables normalized to $2k_B T_e$; second, B_{IJ} (and W_{IJ}) is, at most, a function of positions (and not of velocities); and third, the tensorial fluctuation-dissipation theorem must hold [39]:

$$\mathsf{B}_{IJ} = \sum_K \mathsf{W}_{IK}\mathsf{W}^{\mathrm{T}}_{JK}. \tag{2}$$

Specific choices of W_{IJ} (and U_{adiab}) and its parametrization are given later.

The objective of our paper is to develop a model for the second term in Eq. (1) based on *ab initio* calculations of the coupling between ion and electrons over a wide range of energies and ion configurations, and apply it to describe a full calculation of the collision process. We separate this work in two papers; in this Part I, we report on the *ab initio* methodology used to translate stopping power, a complex quantum mechanical result, into a functional form well suited for the implementation into classical MD; namely, to find explicit expressions for the B_{IJ} function appearing in the second term of Eq. (1) while simultaneously preserving a correct correspondence with W_{IJ} appearing in the third term. Part II, to be published, addresses the nonadiabatic ion dynamics applying our modified Langevin dynamics [39] with the dissipation functions developed here, providing a full picture from the ballistic to the thermal phases of a collision cascade.

III. FIRST-PRINCIPLES ELECTRON DYNAMICS

A. Time-dependent density-functional theory

To study deviations from the BOA, we introduce a specific quantum mechanics framework, namely *ab initio* nonadiabatic TDDFT for electrons [29] combined with Ehrenfest dynamics for the ions [36]. This parameter-free method used to model electronic excitations is particularly suitable in the presence of substantial electronic excitations and in the limit where ions behave classically; it opens a window to observe the microscopic dynamics and dissipative effects for arbitrary configurations, with unprecedented detail and accuracy.

In this theory, single-electron states evolving in time are represented by electron wave functions $\{\psi_i\}$ in a periodic supercell interacting in a mean-field effective potential produced by other electrons and ions; wave functions are the solutions of these time-dependent equations,

$$i\hbar\frac{\partial}{\partial t}\psi_i(\mathbf{r},t) = \left\{-\frac{\hbar^2\nabla^2}{2m_e} + V_{\mathrm{ext}}[\{\mathbf{R}_J(t)\}_J](\mathbf{r}) + V_{\mathrm{int}}[n](\mathbf{r})\right\}\psi_i(\mathbf{r},t), \tag{3}$$

where V_{ext} is the external potential produced by ions $\{\mathbf{R}_J(t)\}$ and V_{int} is the Hartree and exchange-correlation potential for the spatial-dependent electron density n.

When ions move, the energy deposited into the electronic system above its instantaneous GS represents the work done by nonconservative forces.

The practical utilization of TDDFT has the same system-size limitations of DFT (e.g., hundreds of atoms) and time scales limited to a few femtoseconds. These limitations prevent the utilization of TDDFT in full or even the smallest meaningful collective ionic events (e.g., collision cascades); however, systems modeled here are large enough to extract the parameters for coarser models of the dissipative dynamics.

Due to the limitations mentioned above, the framework expressed here requires a selection of a special set of well-controlled trajectories in small systems from which the full classical dissipative model can be adjusted. There are at least three representative trajectories that are relevant to the problem of cascades: (i) ions (e.g., primary knock-on atoms, PKAs) channeling or moving interstitial in the lattice in which a specific ion (projectile) travels ballistically through at least several unit cells, (ii) head-on or binary collision in which specific pairs of projectile and host atoms approach each other (low impact parameter) at high energies, and (iii) ions at their lattice positions oscillating at typical phonon frequencies and exchanging, near equilibrium, energy with electrons.

Our set of *ab initio* TDDFT simulations are based on representatives of these types of trajectories in rather small systems. The idea is that a model for nonadiabatic forces will be considered adequate if it can reproduce the TDDFT dissipative forces (friction terms) in this set of selected trajectories. The materials of interest are the $3d$ transition metals known to form single-phase fcc-concentrated solid solutions, namely Ni, Co, Fe, and Cr [37]. As we shall see, the nature of the model calls for its parametrization via simulations of *each* element in a representative host.

Two types of first-principles electronic calculations are performed; one is the adiabatic or BOA [1], in which electrons are always at their GS, i.e., standard DFT calculations. The other method is TDDFT, in which electrons evolve in time from their GS at time $t = 0$ [29]. Both types of simulations were performed using the plane waves Lawrence Livermore code Qball (for details, see Refs. [42,43]) with norm-conserving pseudopotentials and an energy cutoff of 150Ry for the plane-wave basis set. The calculations include $3p$ semicore states, are nonmagnetic, and use the adiabatic LDA exchange-correlation potential [44].

For all projectile trajectories, a supercell with 108 atoms on a fcc lattice with a lattice parameter of 3.52 Å was used, with a projectile velocity of 0.3 a.u. (131keV for Ni), kept constant while the target atoms are at rest, i.e., we do not integrate the equation of motion of any target atom in the simulation: The projectile is forced to have a rectilinear trajectory at constant velocity. This method simplifies the analysis of the relevant information; it then represents an open system where energy is given to or subtracted from the projectile to keep its velocity constant.

A point needs to be made justifying the use of a small supercell geometry. Periodic boundary conditions in our simulations imply that an array of projectiles with parallel trajectories separated by 10.56 Å interact simultaneously with the target; projectile-projectile interactions may therefore affect the results. However, in metals the screening length is of the order of the nearest-neighbor distance, restricting the perturbation caused by the projectile to its local surroundings.

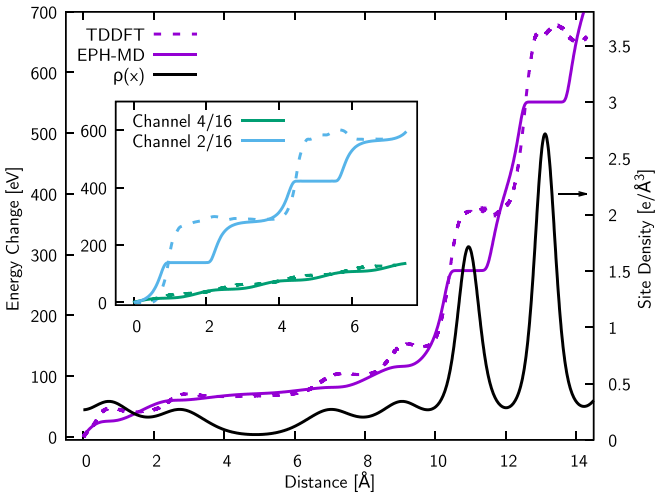

FIG. 1. Energy transfer to the electronic system by a Ni projectile traveling in fcc Ni at $v = 0.3$ a.u., along three different trajectories. The dashed lines are obtained from TDDFT calculations and solid lines from the fitted MD model. The main plot represents the incommensurate trajectory where the site density is also added for informative purposes. The subset shows the energy transfer along the channel in the center (channel 4/16) and offset from the channel (channel 2/16).

This effect can be seen in the fact that the stopping power process is basically a two-body effect involving the projectile and its closest target atom, as Figs. 4 and 5 in Ref. [45] and discussions therein prove.

Our model is constructed for a bounded set of velocities (less than 1 a.u.), mainly because we limit electronic excitations to $3p$ semicore states. Given that bound, the question is whether the cell is large enough to be in the limit of effective screening between replicas (and their wakes). Size effects in the limit of large velocity can be estimated, as we do in Ref. [46]. Here, we made sure that the results are converged with respect to the cell size. Independent support to this assertion comes from Ref. [47]; Fig. 1 in that paper shows that the screening decays only after the maximum stopping is achieved. In the case of Ni into Ni, the maximum of stopping occurs at velocities around 10 a.u., well above the upper limit of validity of our model. Our case is not $|Z| = 1$ like in this analytic model, but at the same time, more (semicore) electrons participate in the screening as shown in Ref. [34], so the argument holds.

Similarly, time effects for a fixed cell size and velocity imply that there will be a time after which the energy deposition is no longer an intensive quantity. In the same way that we have access to finite size effects (for bounded velocity) by increasing the cell size, we have access to the time domain question by running long enough to reach a steady state and observe the saturation of the energy deposition later on. Longer times in our simulation cell are obtained when the projectile wraps around the cell and reenters. As an example of a stationary state, from Fig. 1 it can be seen that at each equivalent two-body encounter in a given trajectory, the energy deposited into electrons is essentially the same, indicating no saturation effects. Also, we note that after one passage of the projectile across the entire sample, the total energy deposited into the target is a few hundred eV. The system contains (109 x 16) 1744 electrons, which means that less than half an eV/electron is deposited; this is a small amount in terms of the band energy of the electrons. A pictorial illustration of this effect is shown in Fig. 8 of Ref. [48].

The difference in energy between TDDFT and BOA calculations for the same trajectory represents the net energy given to electrons by the projectile, i.e., energy that would not be given to the electrons if the ions move adiabatically. Therefore, this energy difference is the nonadiabatic part of the problem.

It is important to note that, contrary to perturbative approaches to electronic stopping, adiabatic DFT and nonadiabatic TDDFT formalism do not require an *a priori* choice of the charge state for the projectile. In all simulations, the total nuclear charge of the 108+1 ions is exactly compensated by the same number of electrons, i.e., the sample is electrically neutral. As the projectile moves, the effective charge that moves with it is part of the solution to the calculation, and not an input. Analysis of the charge states of the projectile and of the closest target atoms for similar channeling simulations can be found in Ref. [49].

B. Simulation results

We run TDDFT and BOA simulations for two cases, namely, a Ni projectile into a Ni target, and Ni, Co, Fe, and Cr projectiles into a NiCoFeCr alloy target.

1. Ni projectile into Ni target

As a first example, and since Ni is special among other elements in a recently discovered family of fcc-concentrated solid solutions [37], we start by describing the case of a moving Ni ion (projectile) in a Ni host (target). The Ni projectile moves through a pristine 108/107-atom system along three types of trajectories, two ⟨001⟩ channeling directions, one at the center of the channel (projectile Cartesian position along $\mathbf{r}(t) = (4/16a_0, 4/16a_0, vt)$, and another off-center $\mathbf{r}(t) = (2/16a_0, 2/16a_0, vt)$, and one incommensurate direction close to the ⟨111⟩ direction, which includes going through a *vacancy*, introduced purposely to explore dissipation at the lowest host electronic density, representative of the e-ph interaction regime. The chosen value for v in these simulations is 0.3 a.u., which allows obtaining a clear numerical result for dissipation; the results for lower velocities are down-extrapolated as linear in the velocity by the model. This is a relatively low velocity in terms of deviations from linearity of stopping power and validity of the pseudopotential approximation [34].

From the derivative of the energy difference between TDDFT and BOA runs, we extract the local stopping power as a function of position along the trajectory, which is used as input for adjusting the dissipation model. With dashed lines, Fig. 1 shows $E_{\mathrm{TDDFT}}(r) - E_{\mathrm{BOA}}(r)$, the energy transferred from the moving projectile to the electronic system up to a distance r along the trajectory for the two channeling directions (inset) and for the incommensurate direction (main panel). The stepwise structure of these curves reflects the projectile

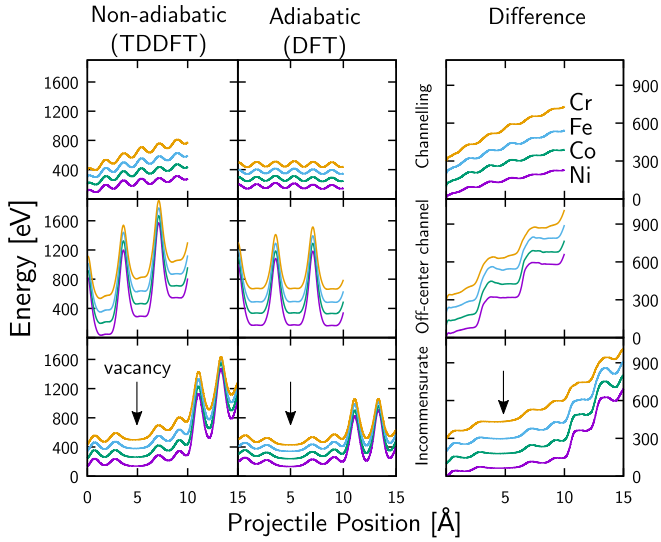

FIG. 2. Electronic energy as a function of projectile position for Ni (black), Co (green), Fe (blue), Cr (yellow) projectiles at $v = 0.3$ a.u. along rectilinear trajectories. Left column: Total nonadiabatic electronic energy. Center column: Adiabatic or BOA electronic energy. Right column: Difference between them. Top row: Along ⟨100⟩ direction passing at the center of the channel. Center row: "Off-center" along ⟨100⟩ direction with an impact parameter of 1.19 a.u. from closest atoms at the channel. Bottom row: Along an incommensurate direction starting at the center of a ⟨100⟩ channel. The target is a quasirandom solid solution alloy of equiatomic NiCoFeCr.

close encounters with the target atoms. This figure also shows the fitting to these curves by our model, which we discuss later. Finally, Fig. 1 also shows the host GS electronic density (lowest curve and right y axis), which will be used to relate stopping power to electronic GS density.

2. Ni, Co, Fe, Cr projectiles into a NiCoFeCr target

Similarly, we run TDDFT and BOA simulations of self-irradiated NiCoFeCr, as representative of a concentrated solid solution. The initial structure was taken from our previous work [50], where we found that there exists a degree of short-range order in this system. We studied the same nominal trajectories described above in the underlying fcc lattice. Clearly, our strategy explores only a few of all possible environments a projectile may find in a random solid solution, but we assume that the sampling is good enough to extract a dissipation function that represents well the real case.

As we studied four projectile types and three directions on the alloy target, we performed a total of 24 independent simulations. The raw data is presented in Fig. 2, where the electronic energy as a function of projectile position for Ni, Co, Fe, and Cr projectiles versus position along rectilinear trajectories is shown. The three columns represent the total nonadiabatic electronic energy, the adiabatic or BOA electronic energy, and the difference between them, respectively. Each of the three rows show the trajectories studied along ⟨100⟩ direction passing at the center of the channel, "off-center" along ⟨100⟩ direction with a smaller impact parameter of 1.19 a.u. from closest atoms to the channel, and along an incommensurate direction close to ⟨111⟩ starting at the center of a ⟨100⟩ channel, respectively.

The energy transferred to electrons in the case of the four types of projectiles in a fcc NiCoFeCr target is shown in Fig. 3 together with the GS electronic density seen by the projectile along the trajectories, and the results of the dissipation model that we discuss later.

IV. CONSTRUCTION OF THE DISSIPATION MODEL

A. Electronic density

Purposely, electronic density plays an important role in defining the model of local dissipation, which by construction is an explicit function of the electronic density in the vicinity of each moving ion, as envisioned in Ref. [33]. The explicit dependency on the density allows us to define the dissipation function in a wide range of possible local environments.

The data shown in the previous section is used to create the functions that relate the strength of the dissipation to the local electronic density of the host, i.e., part of the B_{IJ} function appearing in the second term of Eq. (1).

Since the goal is to develop a model to be used in classical MD, with no access to instantaneous self-consistent electronic densities, *in lieu*, we use spherical atomlike densities of isolated atoms (obtained here from the OPIUM DFT pseudopotential generation code [51]). This step is necessary because during a classical MD simulation, there is no access to the full self-consistent density solved in the TDDFT code. In a MD simulation, the host electronic density will therefore be calculated as a superposition of spherical atomic densities of atoms close to the moving atom whose electronic friction is being calculated.

Atomic density calculations are done for all four elements (Ni, Co, Fe, Cr) studied in this paper, and the results are tabulated for later use in the MD code, Part II of this work. To control the computational cost of the classical MD simulations, the densities are modified with a cutoff function to ensure they go smoothly to zero at a cutoff distance (5.0 Å). The resulting radial electronic density functions used for individual elements are plotted in Fig. 4.

Atomic densities play two roles in the model, first they define pair correlations of the nonadiabatic forces to provide local conservation of linear and angular momentum, and second partial sum of neighboring atomic densities scale the strength of the local dissipation. Of these roles, the former, as demonstrated in Ref. [39], ensures a rich electron-phonon interaction regime; in particular, it provides different phonon lifetimes for different phonon polarization, while the latter allows us to connect the low-energy regime (electron-phonon equilibration) with the high energy regime (electronic stopping power) under the umbrella of a single model. The model was set up such that only a few functional parameters are free; we assume spatial pair correlations controlled by the functional form of the electronic densities. The main work is focused on defining a local dissipation function as a function of the density.

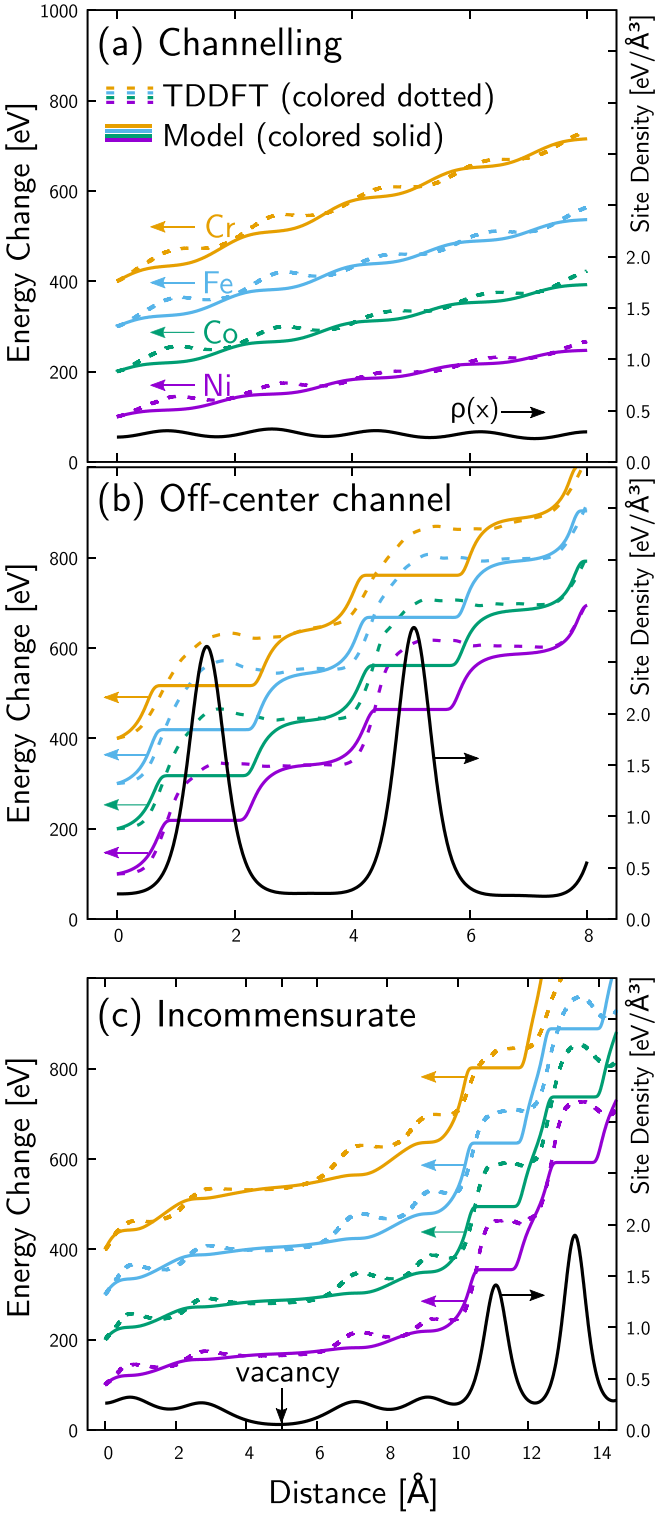

FIG. 3. Energy transfer to electronic system as four different projectiles travel along three different trajectories through NiCoFeCr alloy. Also shown are electronic site densities (solid black line) along the trajectories. The element types selected for projectiles are Ni (purple), Co (green), Fe (blue) and Cr (yellow), with arbitrary vertical offsets. The trajectories studied are (a) channelling (4/16), (b) off-center channel (2/16), and (c) incommensurate. The data plotted with colored dotted lines are obtained from TDDFT calculations and the MD model predictions are shown with colored solid lines.

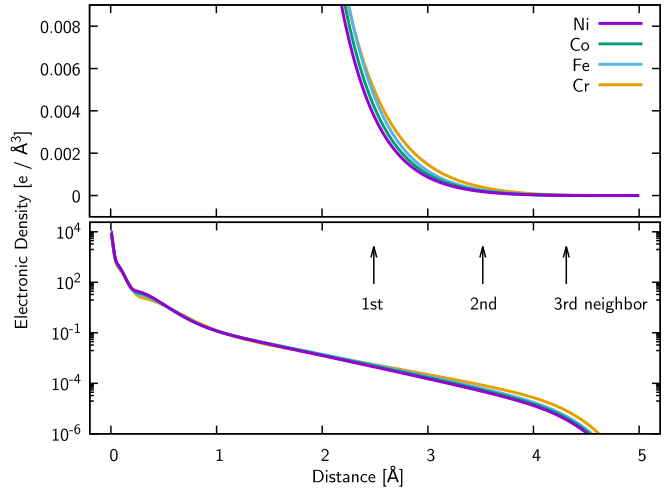

FIG. 4. Electronic density as a function of distance to the nucleus calculated for isolated atoms in vacuum, used for approximating electronic densities along the trajectory of projectiles in our model.

In summary, electronic density defines the geometrical aspect of the model and gives an explicit dependency of the magnitude of dissipation forces (for details, see Ref. [39], and Supplemental Material therein):

$$\mathsf{W}_{IJ} = \begin{cases} -\alpha_J(\bar{\rho}_J)\frac{\rho_I(r_{IJ})}{\bar{\rho}_J}\mathbf{e}_{IJ}\otimes\mathbf{e}_{IJ} & (I\neq J) \\ \alpha_I(\bar{\rho}_I)\sum_{K\neq I}\frac{\rho_K(r_{IK})}{\bar{\rho}_I}\mathbf{e}_{IK}\otimes\mathbf{e}_{IK} & (I=J), \end{cases} \tag{4}$$

where $\bar{\rho}_I = \sum_{J\neq I}\rho_J(r_{IJ})$. Note that this tensor fully defines B_{IJ} by the relation given in Eq. (2). This part of the model, which completes Eq. (1), fully specifies the equations of motion for the ions, which is implemented by us as the USER-EPH *fix* (plug-in) [52] for the LAMMPS code [53]. The remainder of the paper explains the method to adjust the functional parameter $\alpha_I(\rho)$ for each of the four species considered here.

B. Dissipation function

We are interested in deriving an expression for the dissipation of ionic kinetic energy into the electronic system able to capture the complexity implicit in an interaction that covers nine orders of magnitude in energy (from meV to MeV) and ~two orders of magnitude in the local electronic density visited by the moving particle, while at the same time we aim at a model simple enough so it is usable in classical molecular dynamics simulations with the correct asymptotic equilibration limits. These constraints force us to make some simplifications.

In connection with our goal of relating the strength of the dissipation force to the host unperturbed electronic density ρ_0, our previous work [45] shows that, contrary to the meV e-ph interaction regime that can be represented as a stopping process with a dissipative force proportional to the velocity and function of the electronic density, $F_{\text{drag}} = -\beta(\rho_0)v$ [35], the higher energy regime cannot be so represented, because β becomes, at the least, a multivalued function of ρ_0. Here, β symbolically represents a scalar version of the B in Eq. (1).

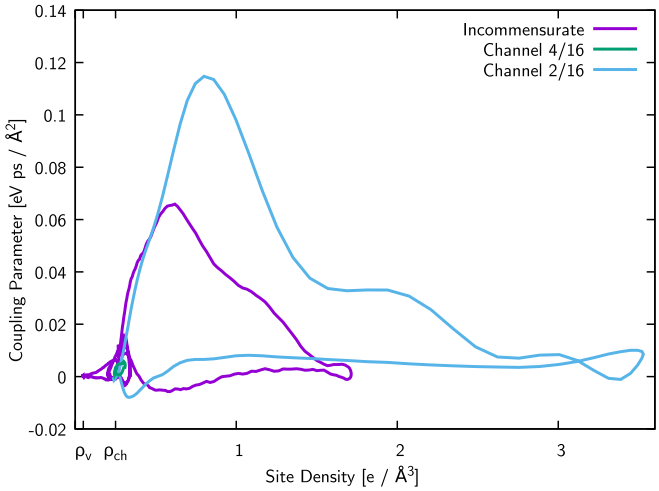

FIG. 5. Coupling parameter $\beta(\rho)$ for a Ni projectile moving with velocity $v = 0.3$ a.u. into a fcc Ni target. The trajectories studied are channelling (4/16), off-center channel (2/16), and incommensurate, as a function of the unperturbed local electronic density ρ_0, from Ref. [45].

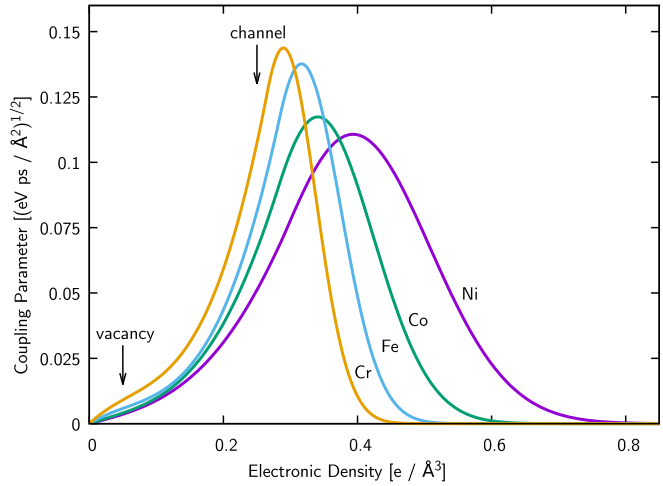

FIG. 6. Dissipation function for each element of interest $\alpha_{\mathrm{Ni,\,Co,\,Fe,\,Cr}}(\rho)$ that parameterizes W_{IJ} in Eq. (4). These functions univocally relate unperturbed electronic density to dissipation, and represent a simplification to the real relationship such as that given in Fig. 5 and in Ref. [45].

Since B is the hermitian square of W [Eq. (2)], the drag coefficient β is dimensionally proportional to α^2.

This multivalued behavior of β is illustrated in Fig. 5, which shows loops when β is represented in terms of ρ_0. In Fig. 1, we reported the energy difference (dashed line), i.e., the energy transferred from the moving projectile to the electronic system, and the host density (solid line) along the projectile trajectory. For example, in that figure one sees two points along the projectile trajectory that have host density equal to $2\ e/\text{Å}^3$. For these points, the derivative of the energy difference divided by the projectile velocity is different; in other words, for a given density there are two different dissipation values β. Therefore, loops appear in the $\beta(\rho)$ representation.

As we explain in Ref. [45], the origin of the multivalued character of $\beta(\rho_0)$ can be traced back to the fact that the GS electronic density seen by the projectile on equivalent points in the incoming and outgoing phases of a collision is the same by symmetry, while the time-dependent density is not. It is then the dynamic response of the electrons during the collision that creates the asymmetry in the dissipation represented as a function of the projectile coordinate, which prevents the construction of an *ad hoc* $\beta(\rho_0)$ (single-valued) functional relation.

For clarity, we highlight here that phonon excitation energies, i.e., meV, originate when ions move close to their crystal equilibrium positions, which coincide with minima of the host electronic density, while high energy collisions, i.e., in the keV–MeV range, bring ions to close contact where they explore regions two or more orders of magnitude higher in electronic density than for the meV case.

The dissipation function will therefore be an average of the loops, chosen to give the same TDDFT total energy dissipation after a full collision, rather than point-by-point agreement with it. To this end, we minimize a fitness function that measures the difference in dissipation between the *ab initio* results and the results obtained by moving a projectile along the same trajectories used in the *ab initio* calculation; the dissipation along these trajectories is calculated using the atomic sphere electronic densities described above and the trial function $\alpha(\rho)$. Note that this is a strong simplification motivated by the practical limitation of resolving the electronic density on the fly. However, compared to other types of bonding, for metals this approximation is reasonable.

The fitting was done separately for each case in which we have *ab initio* data, using the GNU Octave software package with the NLOPT optimization module [54,55], which in turn drove a LAMMPS session with trial parametrizations of the model, and consisted of three stages. First, the function value at the electronic density of a vacancy site, ρ_v, was set so that the electron-phonon coupling strength matches the target values for each case. Next, a cubic spline with six knot points was fitted to reproduce simultaneously the incommensurate and center-channel TDDFT data. Finally, the high-density region of the coupling parameter model was suppressed with an exponential cutoff function. Although intuitively the coupling seems to be an increasing function of the local density, in a physical atomistic system (and also reflected by TDDFT) the electronic excitations in high-density region are suppressed because of the large binding energy of core electrons.

The dissipation functions so obtained are shown in Fig. 6 for the elements of interest in this paper. These figures show that the main difference between the effective coupling and the *ab initio* data is that the former is a function, with absence of loops, i.e., at each density value corresponds a given dissipation (single valued).

V. DISCUSSION AND CONCLUSIONS

In our objective of modeling the nonadiabatic processes involved in energetic ion-solid interactions, we used TDDFT, an *ab initio* technique, to study the energy transferred from moving ions to electrons in a solid both, in the electron-phonon regime (low-energy motion in regions of very low host electronic density), and in the stopping power regime,

where ions come to close contact and overlap large electronic densities. These results show a complex behavior related to the evolution of the electronic structure as electrons are excited. Since our model is to be used in classical MD, with only GS electronic density available in the form of tables, we established a relation between the first-principles result and a simplified model in which the host electronic density seen by the projectile is simply the superposition of atomic densities, and the resulting dissipation is given by a dissipation function that, based on the spherical atom densities, gives the result closest to the *ab initio* one.

The strength and limitations of our model are represented by the similarity between the actual TDDFT dissipation and that predicted by the model, Figs. 1 and 3. We see there that the model is able to predict quite accurately the energy transferred after each collision along the trajectory, but not point by point along the trajectory. This feature was to be expected since we are forced to use frozen, spherical atomic densities and not actual, time-dependent ones. This limitation is the price to pay to have a model that can easily be implemented in classical MD codes at no significant increase in computational cost.

The functions shown in Fig. 6 are the main input for a nonadiabatic MD simulation of collision cascades on alloys and since they provide the coupling strength at all relevant densities, i.e., densities visited by moving atoms at all energies of interest, they will allow the first calculation of the entire collision process, from the ballistic to the thermal phases of a cascade, giving a detailed picture of the energy exchange between ions and electrons till their final thermalization. Such calculation is the goal of our second paper, "Role of electrons in collision cascades in solids. Part II: Molecular dynamics."

ACKNOWLEDGMENTS

Work was performed at the Energy Dissipation to Defect Evolution Center, an Energy Frontier Research Center funded by the U.S. Department of Energy (Award No. 2014ORNL1026). Computing support for this work came from the Lawrence Livermore National Laboratory Institutional Computing Grand Challenge program. Work by A.T. and A.A.C. was performed under the auspices of the U.S. Department of Energy by Lawrence Livermore National Laboratory under Contract No. DE-AC52-07NA27344.

[1] M. Born and R. Oppenheimer, Ann. Phys. **389**, 457 (1927).
[2] A. A. Correa, J. Kohanoff, E. Artacho, D. Sánchez-Portal, and A. Caro, Phys. Rev. Lett. **108**, 213201 (2012).
[3] N. Bohr, Lond. Edinb. Dubl. Phil. Mag. **25**, 10 (1913).
[4] N. Bohr, Lond. Edinb. Dubl. Phil. Mag. **26**, 1 (1913).
[5] N. Bohr, Lond. Edinb. Dubl. Phil. Mag. **26**, 476 (1913).
[6] N. Bohr, Lond. Edinb. Dubl. Phil. Mag. **30**, 581 (1915).
[7] P. Sigmund, Nucl. Instrum. Methods Phys. Res. B: Beam Interact. Mater. Atoms **406**, 391 (2017).
[8] J. Lindhard and M. Scharff, Phys. Rev. **124**, 128 (1961).
[9] J. Lindhard, V. Nielsen, M. Scharff, and P. V. Thomsen, Mat. Fys. Medd. Dan. Vid. Selsk. **33**, 1 (1963).
[10] J. Lindhard, M. Scharff, and H. E. Schiøtt, Mat. Fys. Medd. Dan. Vid. Selsk. **33**, 1 (1963).
[11] J. Lindhard, V. Nielsen, and M. Scharff, Mat. Fys. Medd. Dan. Vid. Selsk. **36**, 1 (1968).
[12] G. S. Was, *Fundamentals of Radiation Materials Science: Metals and Alloys* (Springer, Berlin, Germany, 2007).
[13] U. Fano, Annu. Rev. Nucl. Part. Sci. **13**, 1 (1963).
[14] P. Sigmund and A. Schinner, Nucl. Instrum. Methods Phys. Res. B: Beam Interact. Mater. Atoms **382**, 15 (2016).
[15] E. E. Quashie, B. C. Saha, X. Andrade, and A. A. Correa, Phys. Rev. A **95**, 042517 (2017).
[16] E. E. Quashie and A. A. Correa, Phys. Rev. B **98**, 235122 (2018).
[17] S. N. Markin, D. Primetzhofer, and P. Bauer, Phys. Rev. Lett. **103**, 113201 (2009).
[18] O. B. Firsov, Zh. Eksp. Theor. Fiz. **36**, 1517 (1959) [Sov. Phys. JETP **9**, 1076 (1959)].
[19] W. D. Wilson, L. G. Haggmark, and J. P. Biersack, Phys. Rev. B **15**, 2458 (1977).
[20] J. F. Ziegler, J. P. Biersack, U. Littmark, and H. H. Anderson, *The Stopping and Ranges of Ions in Matter* (Pergamon, Oxford, UK, 1985).
[21] J. H. Ormrod and H. E. Duckworth, Can. J. Phys. **41**, 1424 (1963).
[22] Y. Miyamoto and H. Zhang, Phys. Rev. B **77**, 161402(R) (2008).
[23] S. Bubin, B. Wang, S. Pantelides, and K. Varga, Phys. Rev. B **85**, 235435 (2012).
[24] A. V. Krasheninnikov, Y. Miyamoto, and D. Tománek, Phys. Rev. Lett. **99**, 016104 (2007).
[25] J. M. Pruneda, D. Sánchez-Portal, A. Arnau, J. I. Juaristi, and E. Artacho, Phys. Rev. Lett. **99**, 235501 (2007).
[26] M. A. Zeb, J. Kohanoff, D. Sánchez-Portal, A. Arnau, J. I. Juaristi, and E. Artacho, Phys. Rev. Lett. **108**, 225504 (2012).
[27] I. Tavernelli, M.-P. Gaigeot, R. Vuilleumier, C. Stia, M.-A. Hervé du Penhoat, and M.-F. Politis, Chem. Phys. Chem. **9**, 2099 (2008).
[28] A. Ojanperä, A. V. Krasheninnikov, and M. Puska, Phys. Rev. B **89**, 035120 (2014).
[29] E. Runge and E. K. U. Gross, Phys. Rev. Lett. **52**, 997 (1984).
[30] D. M. Duffy and A. M. Rutherford, J. Phys. Condens. Matter **19**, 016207 (2007).
[31] D. M. Duffy, S. Khakshouri, and A. M. Rutherford, Nucl. Instrum. Methods Phys. R es. B: Beam Interact. Mater. Atoms **267**, 3050 (2009).
[32] E. Zarkadoula, G. Samolyuk, and W. J. Weber, AIP Adv. **8**, 015121 (2018).
[33] A. Caro and M. Victoria, Phys. Rev. A **40**, 2287 (1989).
[34] R. Ullah, E. Artacho, and A. A. Correa, Phys. Rev. Lett. **121**, 116401 (2018).
[35] A. Caro, A. A. Correa, A. Tamm, G. D. Samolyuk, and G. M. Stocks, Phys. Rev. B **92**, 144309 (2015).
[36] P. Ehrenfest, Z. Phys. **45**, 455 (1927).
[37] Y. Zhang, G. M. Stocks, K. Jin, C. Lu, H. Bei, B. C. Sales, L. Wang, L. K. B'eland, R. E. Stoller, G. D. Samolyuk, M. Caro, A. Caro, and W. J. Weber, Nat. Commun. **6**, 8736 (2015).
[38] P. Langevin, C. R. Acad. Sci. Paris. **146**, 530 (1908); reviewed by D. S. Lemons and A. Gythiel, Am. J. Phys. **65**, 1079 (1997).

[39] A. Tamm, M. Caro, A. Caro, G. Samolyuk, M. Klintenberg, and A. A. Correa, Phys. Rev. Lett. **120**, 185501 (2018).
[40] M. Head-Gordon and J. C. Tully, J. Chem. Phys. **103**, 10137 (1995).
[41] M. Askerka, R. J. Maurer, V. S. Batista, and J. C. Tully, Phys. Rev. Lett. **116**, 217601 (2016).
[42] F. Gygi, IBM J. Res. Dev. **52**, 137 (2008).
[43] E. W. Draeger, X. Andrade, J. A. Gunnels, A. Bhatele, A. Schleife, and A. A. Correa, J. Parallel Distrib. Comput. **106**, 205 (2017).
[44] The use of the term adiabatic here refers to the usual approximation in TD-DFT of not considering XC potential with memory effect. It is not to be confused with the discussion about nonadiabatic behavior between ions and electrons, the subject of this paper.
[45] M. Caro, A. Tamm, A. A. Correa, and A. Caro, J. Nucl. Mater. **507**, 258 (2018).
[46] A. Schleife, Y. Kanai, and A. A. Correa, Phys. Rev. B **91**, 014306 (2015).
[47] B. Nersisyanab, J. M. Fernández-Varea, and N. R. Arista, Nucl. Instrum. Methods Phys. Res. B: Beam Interact. Mater. Atoms **354**, 167 (2015).
[48] A. A. Correa, Comput. Mater. Sci. **150**, 291 (2018).
[49] M. Caro, A. A. Correa, E. Artacho, and A. Caro, Sci. Rep. **7**, 2618 (2017).
[50] A. Tamm, A. Aabloo, M. Klintenberg, M. Stocks, and A. Caro, Acta Mater. **99**, 307 (2015).
[51] J. Yang, Opium—Pseudopotential Generation Project (2018), http://opium.sourceforge.net.
[52] LAMMPS: Large-Scale Atomic/Molecular Massively Parallel Simulator is a classical molecular dynamics code, http://lammps.sandia.gov, utilized here in combination with USER-EPH a custom developed package for parameterized electron-phonon coupling, http://github.com/LLNL/USER-EPH.
[53] S. Plimpton, J. Comput. Phys. **117**, 1 (1995).
[54] S. G. Johnson, The NLopt Nonlinear-Optimization Package (2018), http://ab-initio.mit.edu/nlopt.
[55] J. W. Eaton, D. Bateman, and S. Hauberg, *GNU Octave Manual Version 3* (Network Theory Ltd., UK, 2008).